Supporting Information

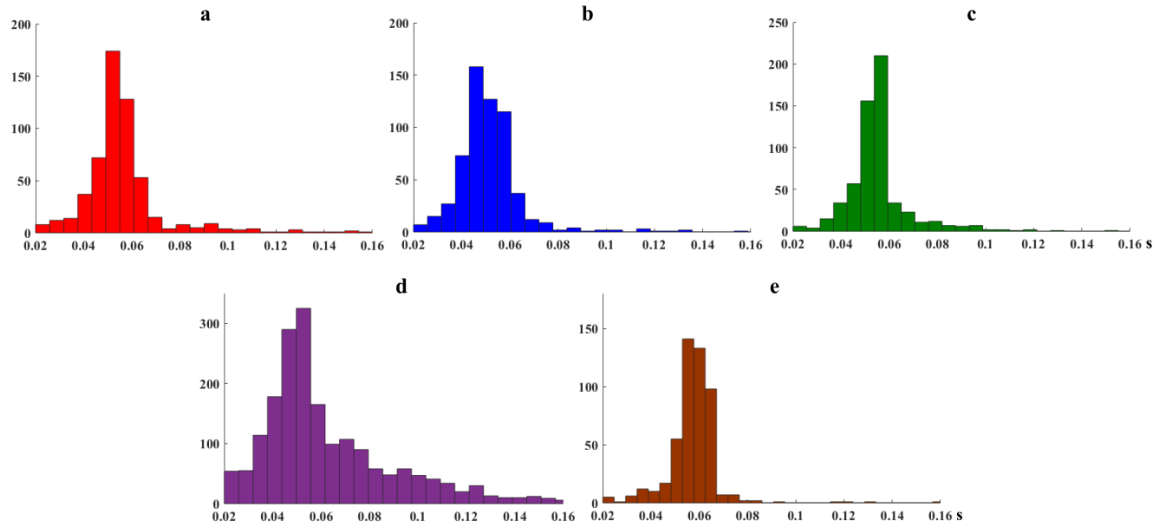

Figure S1: Histograms of the estimated T_2* values from all five training data. Note that T_2* values less than 20 ms or larger than 200 ms were filtered out, thus the different numbers in each bin for different data.

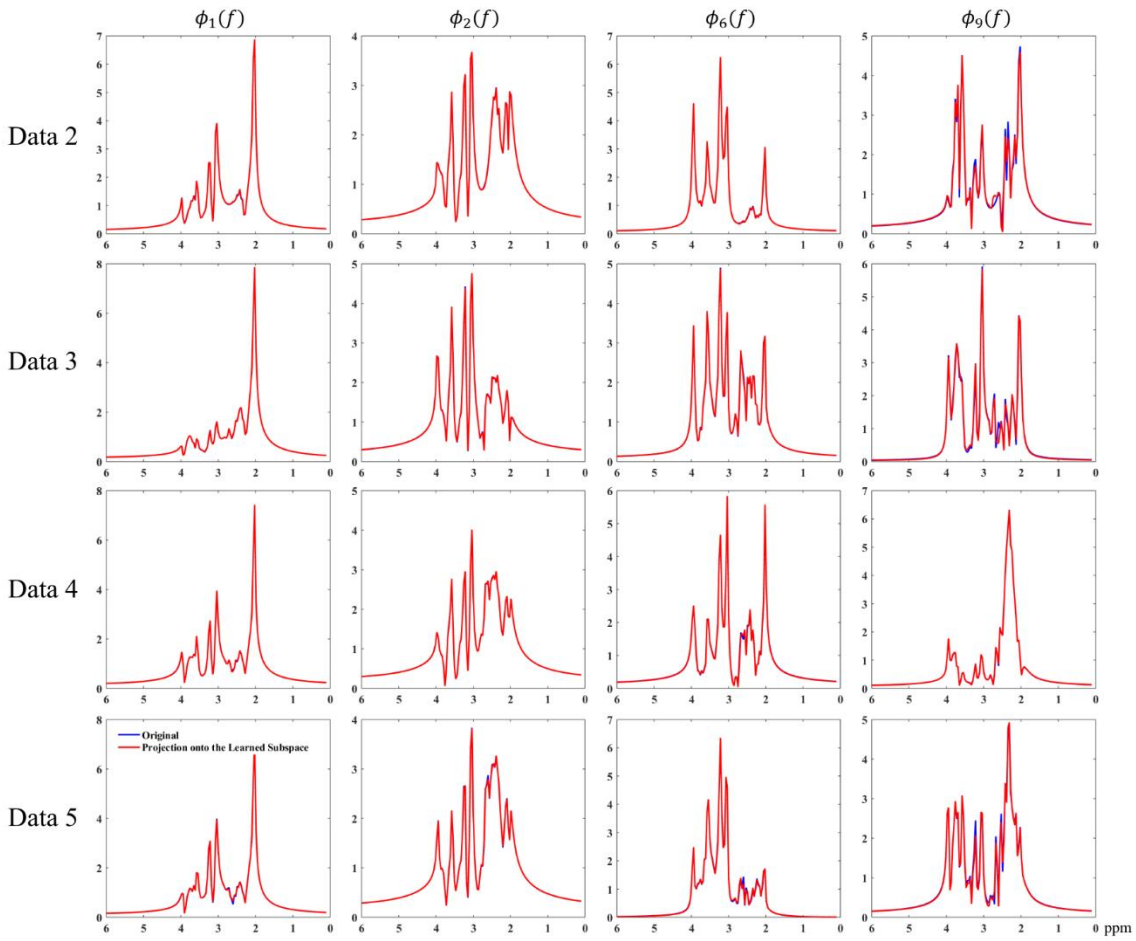

Figure S2: A "leave-one-out" comparison of the subspace estimated from a single training data and the subspace learned from the remaining four. The spectral basis functions from individual training data and their projections onto the subspace learned from other four are shown in different rows. The projection errors are 4.5%, 4.1%, 3.5% and 5.8% for data 2, 3, 4 and 5, respectively. The same result for data 1 has been shown in the main text.

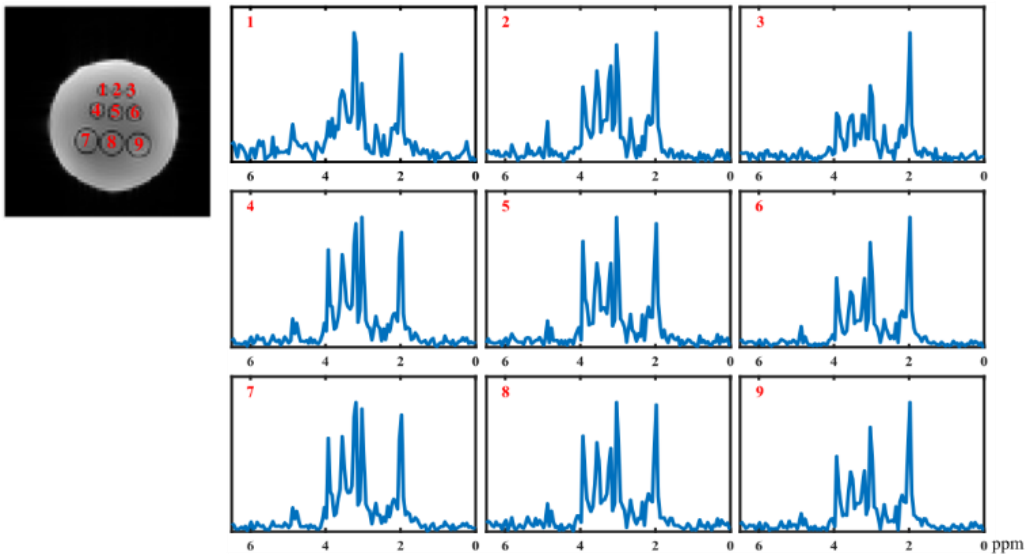

Figure S3: Representative spatially-resolved voxel spectra from different vials in the phantom. The nominal voxel size is 2.6x2.6x3 mm^3 and the locations are marked by the numbers in the water image shown on the left.

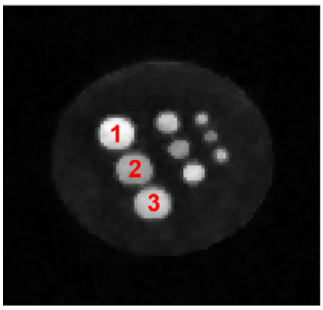

		Vial #1 (C1)	Vial #2 (C2)	Vial #3 (C3)
NAA	Proposed	1.87±0.18	1.16±0.07	1.00±0.07
	Original SPICE	1.88±0.19	1.17±0.07	1.00±0.07
	True	1.875	1.250	1.000
Cho	Proposed	0.64±0.07	0.56±0.06	1.00±0.08
	Original SPICE	0.61±0.06	0.54±0.05	1.00±0.08
	True	0.500	0.500	1.000
mI	Proposed	0.98±0.09	0.82±0.07	1.00±0.07
	Original SPICE	0.92±0.08	0.78±0.07	1.00±0.07
	True	0.800	0.800	1.000

Figure S4: The concentration ratios among different vials for different metabolites in the phantom, using vial #3 as the reference. As can be seen, the ratios between vials for the same metabolite produced by the proposed method (Proposed) and the original SPICE method using data-dependent $\mathcal{D}_1$ (Original SPICE) are very similar, both consistent to the true ratios. There is still room for improvement, e.g., reducing estimation bias, for the lower concentration metabolites.

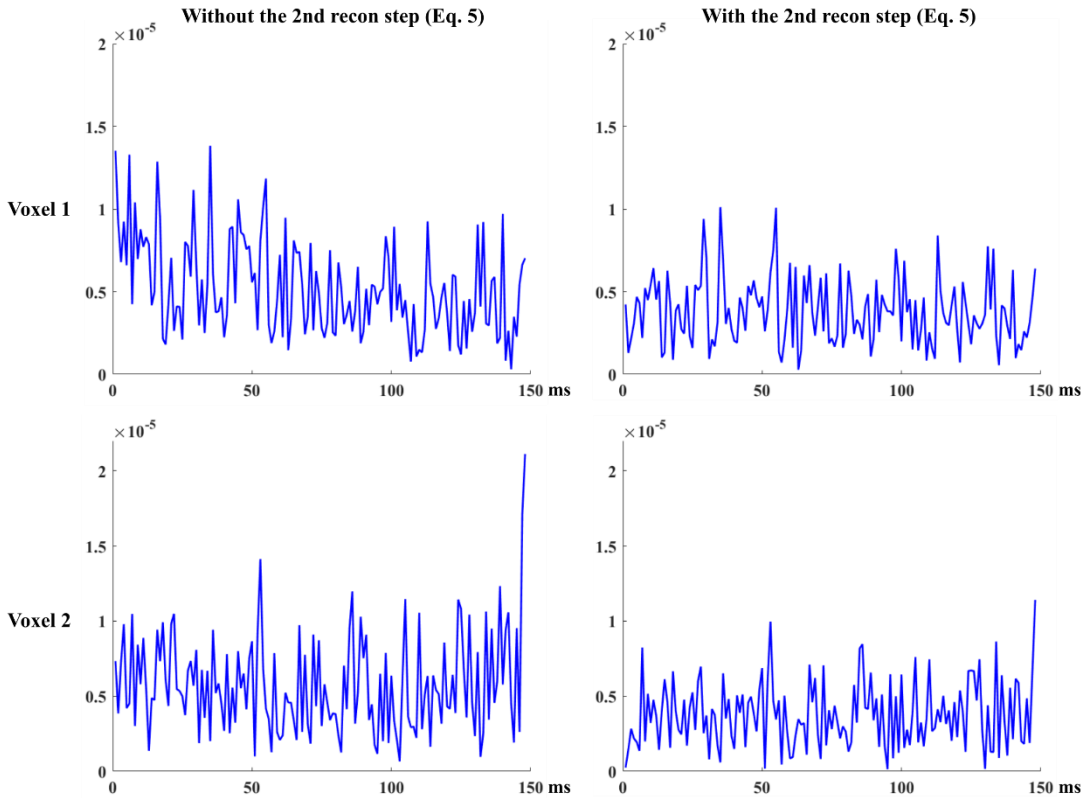

Figure S5: Reconstruction residuals (FIDs) for two selected voxels (shown in different rows). The left column shows the residuals for the reconstruction produced without using the second reconstruction step; the right column shows the residuals for the reconstruction produced using the second step. Structured errors can be observed in the first column which are noticeably reduced in the right column, demonstrating the utility of the second step in improving data consistency and reducing model bias.

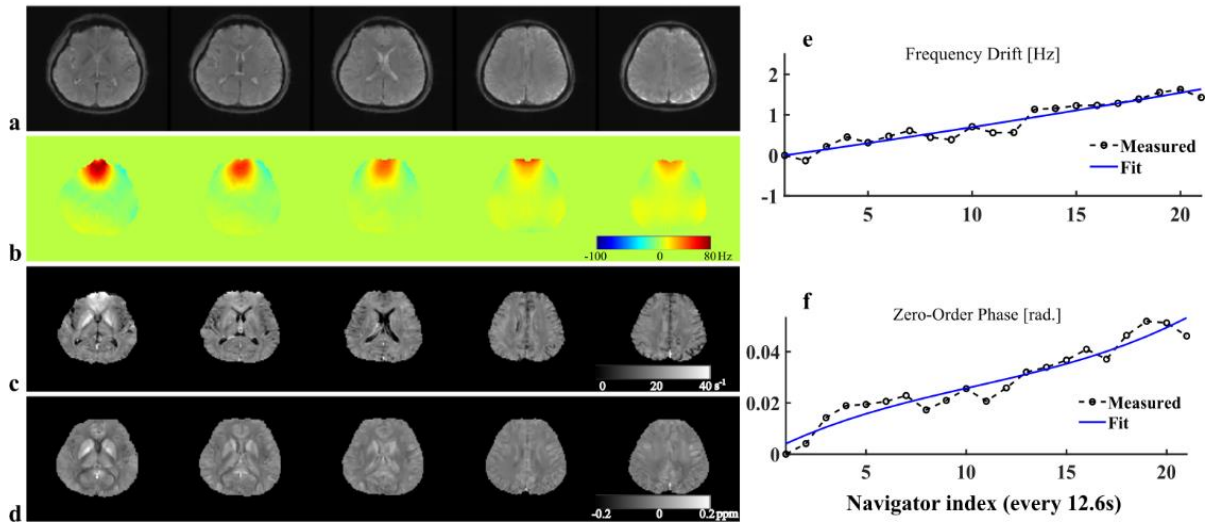

Figure S6: An illustration of various kinds of information that can be extracted from the companion water spectroscopic signal generated by our acquisition: (a) structural images (different echoes will have different mixed T_1 and T_2^* contrasts); (b) B_0 maps; (c) R_2^* maps and (d) tissue susceptibility maps. System instability, such as frequency (e) and phase drifts (f) can be tracked and corrected for using the interleaved navigators.

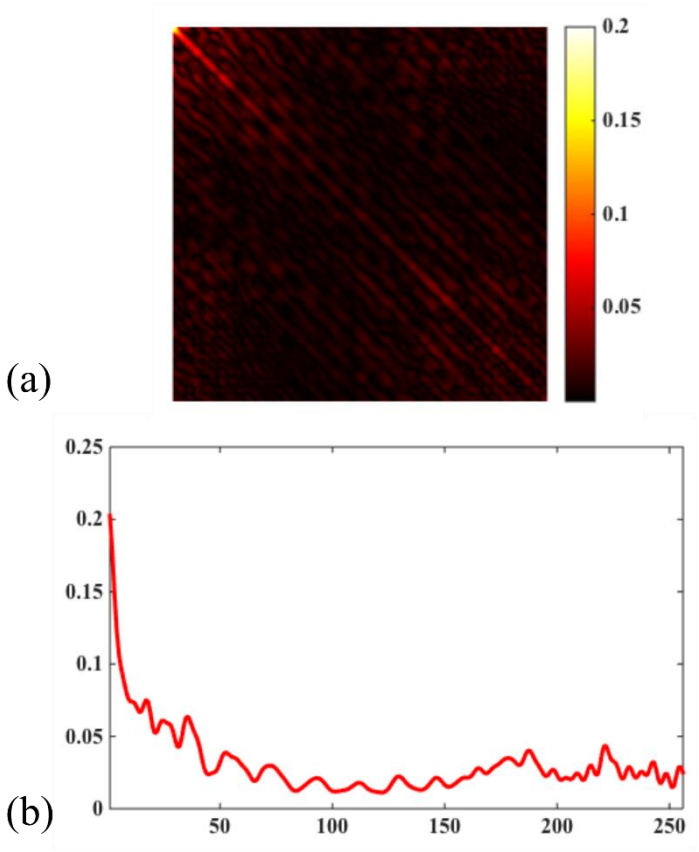

Figure S7: Variance analysis for the subspace constrained reconstruction: (a) Covariance matrix for an individual 256-point FID that underwent the subspace fitting (dimensionality of the subspace was 10). The unit for each element is σ^2, which is the variance of the Fourier reconstruction at individual points; (b) Variances for individual FID points, corresponding to the diagonal elements of the covariance matrix in (a). Significant noise variance reduction can be observed.

Table S1: Comparison of reconstructions using the learned subspace and the subspace estimated from subject/data-specific D_1. Relative l_2 errors between the metabolite maps from the two different reconstructions were calculated and compared in the table below. The results for 5 different datasets were obtained in a leave-one-out fashion.

	Data 1	Data 2	Data 3	Data 4	Data 5
NAA	0.020	0.028	0.041	0.037	0.024
Cr	0.123	0.120	0.093	0.113	0.064
Cho	0.255	0.228	0.126	0.173	0.080
Glx	0.214	0.259	0.139	0.144	0.122
mI	0.121	0.127	0.104	0.154	0.098